A Method to Build Cloud Free Images from CBERS-4 AWFI Sensor Using Median Filtering

Laercio M. Namikawa

National Institute for Space Research
Image Processing Division
Av. dos Astronautas, 1758 São José dos Campos, Brazil

`laercio@dpi.inpe.br`

Abstract. *Cloud free images are useful for applications where the user is more interested in the visual identification of variability of a phenomenon than in the actual values. The presence of clouds and their shadows hinder the visual interpretation in these applications. Median values in data sets are a better representation of the true value than the average when the data set is contaminated with unusual high or low values. Since clouds and their shadows are these unusual values, the median value of a pixel from images gathered in different conditions could provide true representation of the pixel value. To test this hypothesis, images from CBERS-4 AWFI sensor covering an area of 70 Km by 60 km around Brasília in Brazil and acquired from 2017/July/20th to 2017/August/24th were processed using data sets with 3, 5 and 6 images. The results indicate that the smaller set is enough to build a cloud free image where a pixel has at least 2 cloud free data. In more general cases, 6 images are enough to build a cloud free data.*

1. Introduction

Descriptive statistics provide means to understand the contents of a data set. When the data set represents measurements of a phenomenon, descriptive statistics can be used to obtain the most likely value of the phenomena through the measures of central tendency. The most common measures of central tendency are mean, mode and median. When the measurements in the data set are contaminated by spurious values of diverse origins, the mean statistic is appropriate only if these values are randomly distributed around a normal distribution. Mode is defined as the most common value in the data set; therefore, it requires a sufficient number of measurements to be a good representation of the most likely value. When the data set contamination is due to values much higher or lower than the phenomenon expected value, the median statistic decreases the influence of the skewness in the representation of the central value.

In Image Processing, median filters are used to remove random noise and are especially useful for the "salt and pepper" type (Gonzalez and Woods, 2002), where the image is contaminated by unexpected high or low values. The use of median filter is limited to the spatial domain through the use of a "window" that selects the neighborhood of a central pixel to be filtered. The values of the pixels under the window are ranked and the median value replaces the central pixel value. For example, in a 3 rows by 3 columns neighborhood, the 5th element of the ranked values is the new central pixel value. In a similar way to other image processing filters, the median filter

may cause loss of information; however, the benefits of suppressing noisy information counterweigh its impacts.

Optical images acquisition by satellite sensors depends on the amount of solar radiation and on the transmittance of the atmosphere (Richards, 1999). Any presence of contaminants in the atmosphere, such as clouds, will interfere with the image ability to represent the target reflectance. In the presence of clouds, images will be contaminated by pixels with high reflectance values where the clouds are located and also by low reflectance pixels where clouds cast shadows. Figure 1 shows an example of an image with (a) and without (b) clouds.
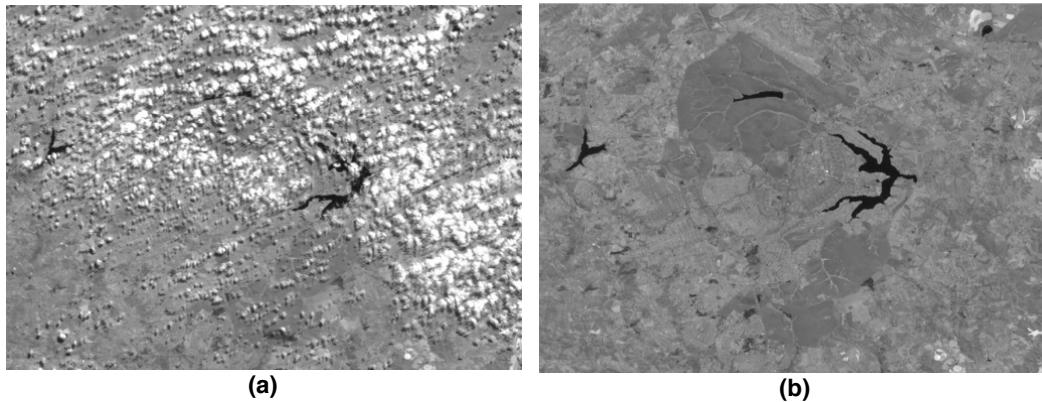

(a)   **(b)**

Figure 1. Example of an image with (a) and without (b) clouds

One must note that information is lost at those pixels affected by clouds, although some information may be recovered where clouds and their shadows are thin, such as, at the edges of clouds. Therefore, to obtain cloud free images, the lost information should be replaced by pixel values from another image where there are no clouds at those pixels locations. This involves identification of areas affected by clouds and their shadows, selection of pixels from another set of images and replacement of pixels at those areas.

The first step is usually accomplished by a cloud mask that is defined by methods such as FMASK (Zhu and Woodcock, 2012). There are several improvements and adaptations of FMASK for other sensors (Zhu *et. al*, 2015; Frantz *et. al*, 2015); however, FMASK is based on probabilities of a pixel being cloud or shadow based on geometry and radiance from several spectral bands. Therefore, FMASK will be less effective with sensors with a small number of spectral bands. The second step can also be accomplished by using FMASK to select pixels that are not "masked" as cloud or shadow pixel in another image and use their values in the third step.

The third step can use a simple replacement method, but the values at the edges between the original image and the replacement pixels may vary due to change in the reflectance of the area between the date of acquisition of the images. To minimize the sharp edge, a blending is applied at these areas, consisting in simple blending methods by a linear interpolation of the values from pixels of the two images (Szeliski, 2006).

The reliance on FMASK to create cloud free images is a weakness since FMASK has to be customized to obtain good results. Figure 2 shows the areas detected by an adaptation of FMASK for CBERS-4 AWFI sensor images. It can be noticed that

FMASK fails to detect shadows which are disconnected from their clouds and that there are areas without clouds near "real" clouds that are masked due to the geometric approach. Since FMASK also relies on a change of values, some areas where there is a high rate of change in the pixel reflectance are identified as clouds.

This paper proposes the use of median filtering in the temporal domain to create cloud free images. As far as the author knows, there are no solutions for this problem using the technique. The following section describes the method and in Section 3, the cloud free images built for images from CBERS-4 AWFI sensor are analyzed. Section 4 presents discussions on the method.

(a)   **(b)**
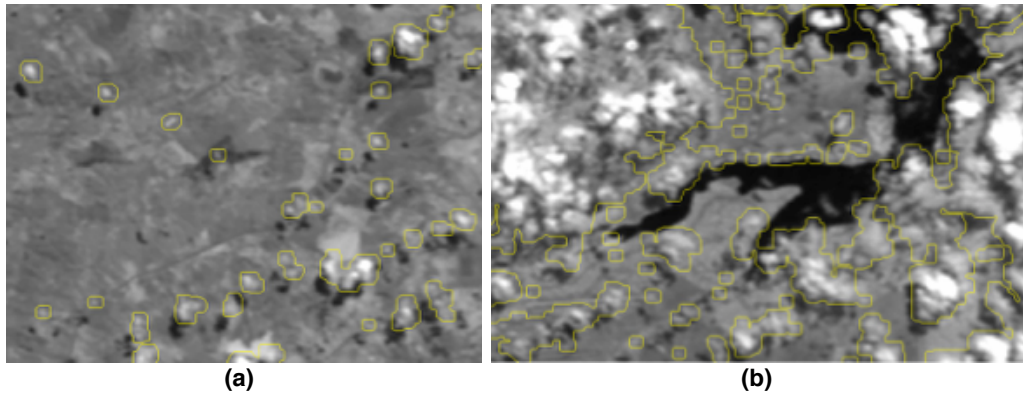
Figure 2. FMASK detected clouds and shadows where detected areas are enclosed by yellow color lines. In (a) shadows are not detected and in (b) some areas are detected as clouds although they are valid targets.

2. Methodology for Using Median to Build Cloud Free Images

In order to combine pixel values from different images, at least two requirements must be met. The first one is that the location of a pixel in one image must be the same location of the pixel on another image, that is, the images must be registered between them with an error of less than one pixel. To ensure that this level of registration quality is met in the example presented here, the images were resampled using a restoration method (Fonseca *et al*., 1993) to a spatial resolution closer to the spatial resolution of the reference image. The reference image is another cloud free image with a spatial resolution better than the images to be combined.

The second requirement is that the pixel values must be "similar". This similarity cannot be guaranteed since the true value of the cloudy (or shadowy) pixel is unknown; however, one can at least guarantee that external factors are eliminated or reduced. The main factor affecting pixel values, which correspond to radiance at the sensor, is the change in the solar irradiation for different acquisition geometries and time/date. The geometry changes how electromagnetic energy reflects from targets and different date/time changes the amount of electromagnetic energy reaching the target. By converting pixel values to reflectance at the Top Of Atmosphere (TOA), changes in pixels values are minimized. To convert pixel values into TOA reflectance, calibration values are used. For CBERS-4 images, PINTO *et al*. (2016) defined the offset and gain required to convert pixel values of MUX and AWFI sensors. Here changes in reflectance due to changes in the target are not considered important, but one must

know how these changes will affect the cloud free images. To minimize this effect, images should be acquired in a short period of time.

Once the requirements are met, the method ranks pixel values of one location for all cloud contaminated input images, and selects the median value to be used in the cloud free output image. Any computer language, either scripting or compiled ones could be used to rank pixel values. In this paper, the LEGAL language (Cordeiro *et al.*, 2009) was used and the code is available at *http://wiki.dpi.inpe.br/doku.php?id=spring: medianpixel*. LEGAL is a map algebra language where each command line represents the processing of the whole image and is implemented inside the SPRING software (available as free open source at *www.spring-gis.org*). In the next Section, the input and the resulting images are analyzed.

3. Images Analysis

The input images for the tests in this paper are from CBERS-4 AWFI sensor. This sensor has a spatial resolution of 64 meters and although the nominal temporal resolution is 5 days, for relatively small areas there are images almost every 3 days. The spectral bands are numbered 13 (visible blue), 14 (visible green), 15 (visible red) and 16 (infrared). The selected area is around Brasília in Brazil and covers a 70 Km by 60 km rectangle. The selected images for this study were acquired by the satellite from 2017/July/20th to 2017/August/24th and obtained from INPE data catalog (*www.dgi.inpe.br/catalog*). Only images covering the whole area were used to avoid mosaicking. Since in this region, these months are mostly dry, 5 of the images are cloud free. Other 5 images have some clouds, with the image from 2017/August/24th being the cloudiest one.

The images were restored to 32 meters spatial resolution and registered using a mosaic of MUX (CBERS-4 20 meter spatial resolution sensor) cloud free images, acquired on 2017/08/15th, 18th, and 21st, as the reference image. Figure 3 shows the band 16 of the images without clouds at then top line (images acquired on 07/23, 08/01, 08/12, 08/15, and 08/18) and the images with clouds in the bottom line (images acquired on 07/20, 07/26, 07/29, 08/09, and 08/24). Band 16 (in the infrared range) was selected to illustrate the method due to its contrast being higher than the other bands.

| 2017/07/23 | 2017/08/01 | 2017/08/12 | 2017/08/15 | 2017/08/18 |

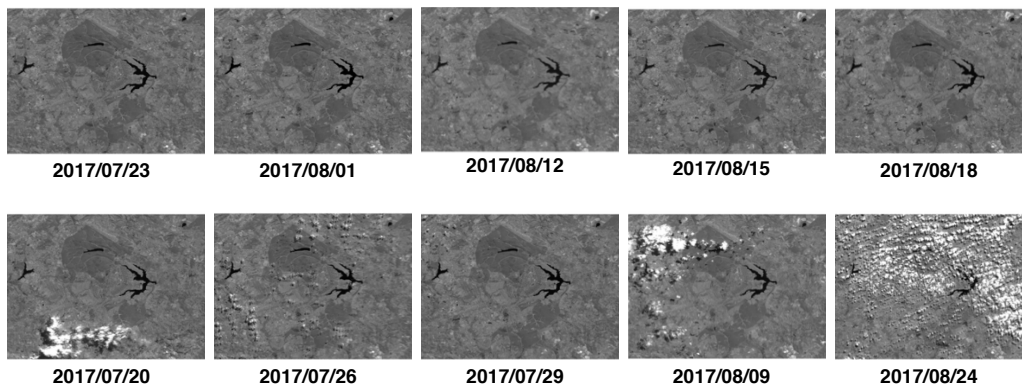| 2017/07/20 | 2017/07/26 | 2017/07/29 | 2017/08/09 | 2017/08/24 |

Figure 3. Images without clouds at the top line and images with clouds at the bottom line. The acquisition dates are under each image. Images are for the infrared band (16) and are contrast stretched.

Mean and standard deviation are measures of image quality. For the set of images used here, cloud contaminated images are expected to have both mean and standard deviation values higher than cloud free ones. Cloud shadows in images are usually smaller than their "source" clouds. Table 1 presents mean and standard deviation values for each image.

Table 1. Mean and standard deviation of available images.

Images Without Clouds			Images With Clouds		
Acq. Date	Mean	Std. Deviation	Acq. Date	Mean	Std. Deviation
Jul/23	20.816	3.466	Jul/20	21.964	6.612
Aug/01	20.936	3.716	Jul/26	21.264	4.967
Aug/12	21.877	3.593	Jul/29	20.755	3.569
Aug/15	21.261	3.616	Aug/09	23.102	7.702
Aug/18	21.352	3.730	Aug/24	26.802	10.530

The analysis confirms these expectations except for the image from 07/29/2017. A closer inspection shows that clouds in this image are small and disconnected from their shadows, which is balancing their low and high values in the mean and standard deviation. Figure 4 shows a small portion of the image acquired on 07/29/2017, where clouds and their shadows can be seen.
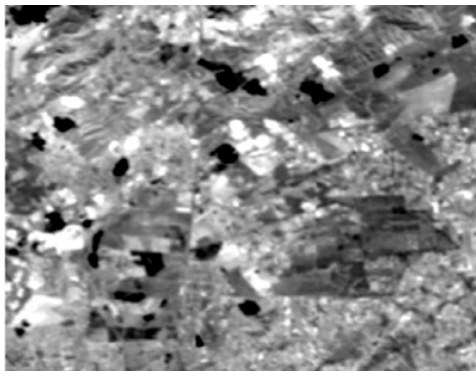

Figure 4. Small portion of the image acquired on 07/29/2017. Clouds are the brightest pixels and their shadows are the darkest ones. Note the separation between clouds and their shadows.

Correlation between images also indicates the quality of an image. In our case, the highest correlation is expected to be between cloud free images that are also closer in acquisition date. Table 2 shows the correlation matrix of all input images. The highest correlation is between images from July/29th and August/1st. The second highest one is between August/12th and 15th. Once again, the image from July/29th is the odd one, but the hypothesis for its behavior has been set previously. The mean correlation between images and cloud free images is shown in the last row and confirms the visual analysis that the lowest quality image is from August/24th, followed by July/20th, August/9th, July/26th and July/29th.

Table 2. Correlation matrix between images. Cloud free images dates are in bold. Values in bold are the highest correlation values and in italic are correlations between all images and cloud free images. Mean correlation in the last row is for the correlation with cloud free images only.

	Jul/20	**Jul/23**	Jul/26	Jul/29	**Aug/1**	Aug/9	**Aug/12**	**Aug/15**	**Aug/18**	Aug/24
Jul/20	1	0.441	0.374	0.438	0.439	0.174	0.413	0.404	0.391	0.024
Jul/23		1	0.789	0.936	*0.958*	0.427	*0.905*	*0.912*	*0.908*	0.218
Jul/26			1	0.784	0.797	0.352	0.761	0.750	0.724	0.186
Jul/29				1	**0.966**	0.432	0.922	0.908	0.871	0.229
Aug/1					1	0.443	*0.937*	*0.928*	*0.906*	0.235
Aug/9						1	0.434	0.436	0.421	0.104
Aug/12							1	***0.965***	*0.926*	0.241
Aug/15								1	*0.959*	0.247
Aug/18									1	0.249
Aug/24										1
Mean	0.418	0.921	0.764	0.921	0.932	0.432	0.933	0.933	0.925	0.238

3.1. Median Image for 3 Input Images

Considering the computational cost of calculating median for each location of the image, one should search for the minimum number of input images. In addition, a small number of input images will also reduce the possibility of a target changing its reflectance. The first test used three input images, all of them with some clouds. The input images and the median (rank order 2) image are shown in Figure 5.
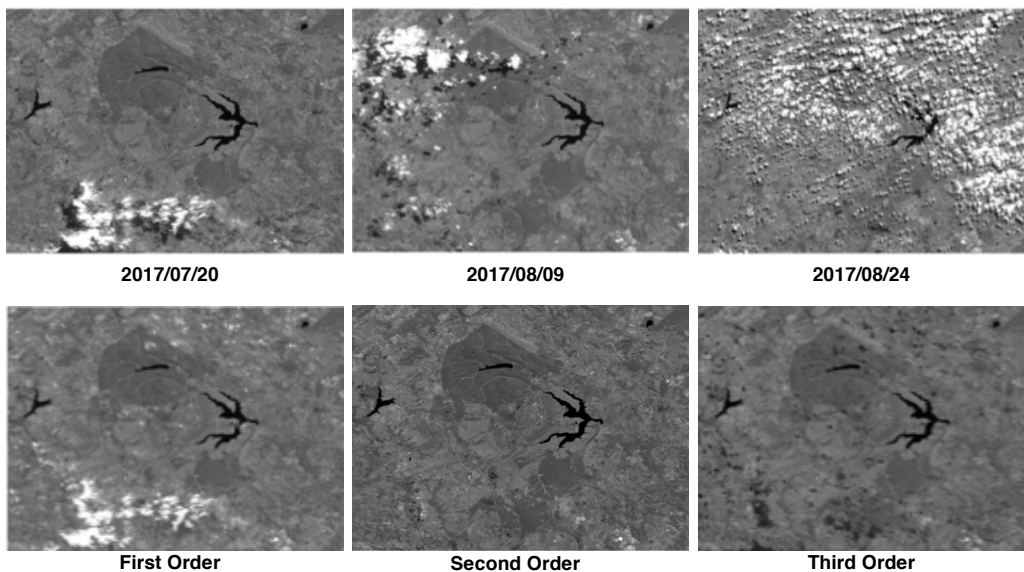

2017/07/20   **2017/08/09**   **2017/08/24**

First Order   **Second Order**   **Third Order**

Figure 5. Images with clouds used to compute median from three images. The acquisition dates and ranking order are under each image.

Figure 5 shows that using three input images remove clouds where only one of the images is contaminated. Areas where there are two pixels with clouds cannot have these pixels replaced by the information from the remaining image.

3.2. Median Image for 5 Input Images

Since a median for 4 input images would not solve the problem when pixels from the same location are contaminated in two images, the next test was considering 5 input images. The test used all five input images contaminated by clouds, all of them with some clouds. The resulting images ranked from 1 (highest pixel value) to the lowest are shown in Figure 6.
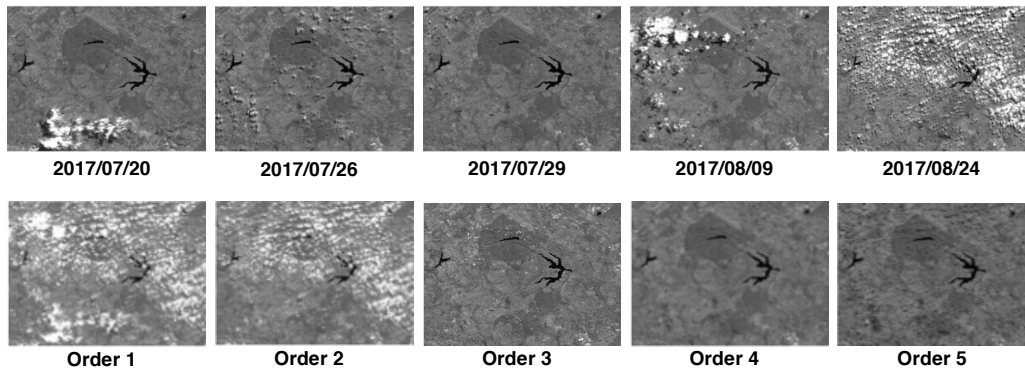

| 2017/07/20 | 2017/07/26 | 2017/07/29 | 2017/08/09 | 2017/08/24 |
| Order 1 | Order 2 | Order 3 | Order 4 | Order 5 |

Figure 6. Images ranked by pixel values at each location. The median image is the order 3 image.

Figure 6 shows that the median image is still contaminated where there are at least three contaminated pixels. The order 4 image shows no contamination by clouds, but there are pixels contaminated by shadows, as presented in Figure 7.
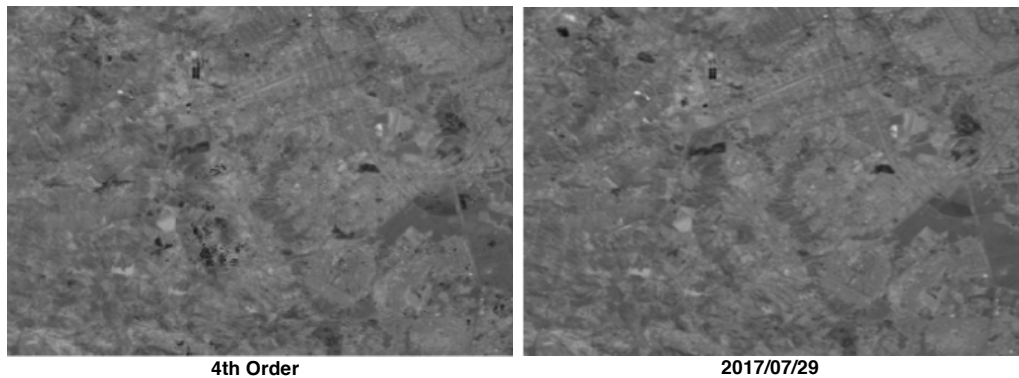

| 4th Order | 2017/07/29 |

Figure 7. Order 4 image zoomed to show pixels contaminate by shadows. These pixels are darker than the cloud free image (in the region) acquired on 2017/07/29.

3.3. Median Image for 6 Input Images

An additional image (acquired on 2017/08/18) was used to test the method. Using a sixth image, which is apparently a cloud free one, the resulting ranked images produces

the third and fourth order images presented in Figure 8. A close inspection reveals that the third order image is still contaminated, but the fourth is not.
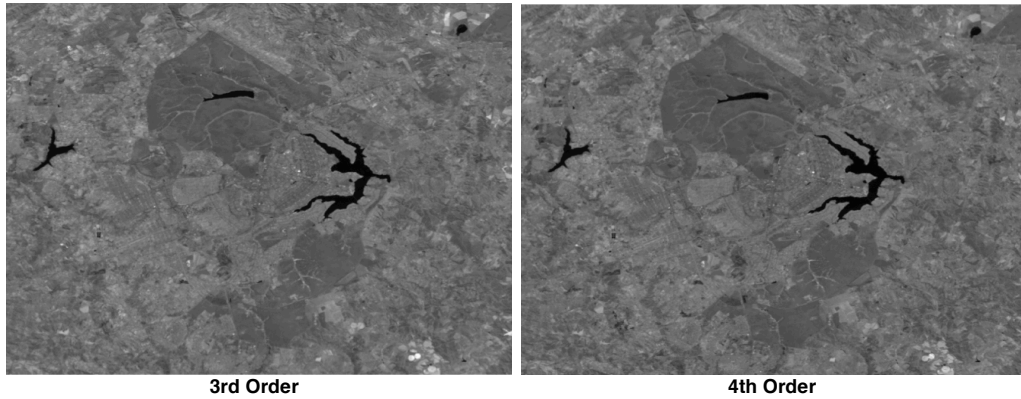

3rd Order **4th Order**

Figure 8. Order 3 and 4 images from 6 input images. Third order image presents some contamination by clouds and fourth order image is cloud free.

In order to verify quantitatively the visual result, correlations between available images and ranked ones were calculated and are presented in Table 3. The highest correlation is for order 4 image and August/1st image. The mean correlation between ranked images and cloud free images shows than the third order image is slightly better than the fourth order. Therefore, there is a quantitative advantage for the third order images that does not capture the visual inspection contamination.

Table 3. Correlation matrix between available images (dates in bold are cloud free images) and ranked images. Value in bold is the highest correlation value and in italic are correlations between ranked and cloud free images.

	First Order	Second Order	Third Order	Fourth Order	Fifth Order	Sixth Order
Jul/20	0.388	0.429	0.470	0.474	0.459	0.386
Jul/23	*0.207*	*0.799*	*0.942*	*0.950*	*0.920*	*0.667*
Jul/26	0.209	0.722	0.803	0.814	0.808	0.669
Jul/29	0.222	0.807	0.947	0.958	0.935	0.679
Aug/1	*0.223*	*0.811*	*0.953*	***0.960***	*0.936*	*0.671*
Aug/9	0.482	0.594	0.457	0.440	0.442	0.394
Aug/12	*0.215*	*0.814*	*0.947*	*0.937*	*0.919*	*0.666*
Aug/15	*0.219*	*0.822*	*0.949*	*0.937*	*0.914*	*0.672*
Aug/18	*0.217*	*0.801*	*0.918*	*0.899*	*0.887*	*0.657*
Aug/24	0.733	0.308	0.252	0.247	0.271	0.364
Mean	0.216	0.809	0.942	0.936	0.915	0.667

The resulting cloud free image (the fourth rank order image) built from 5 cloud-contaminated images and one cloud free image shows that there is no need for more images in this case. In addition, the use of a seventh image would have a much higher computational cost since sorting algorithms are not linear.

4. Concluding Remarks and Future Directions

This paper presented a method to create cloud free images from a set of images that are contaminated by clouds and their shadows. The method relies on the images being registered and ranks pixels of each image by their values. The median value of the pixel is expected to be a cloud/shadow free one. The minimum number of contaminated input images is three; in this case, where pixels are contaminated in one image only, the resulting median image will be cloud/shadow free. Therefore, the number of input images will depend on the distribution of clouds and their shadows in the images. For the test case, this number was 6. In addition, since the number of images is even, when selecting the median, the fourth order image (ranked from brightest to darkest values) is less likely to be cloud/shadow contaminated.

The method will be used to create images for periods of time to be defined. As shown in the test case, for dry season at the Central region of Brazil, cloud free images from CBERS-4 AWFI sensor can be built at least every month, with the possibility of having in the shortest period, one image every 9 days. For other regions and seasons, only a systematic use of the method will define the period.

Since the method uses the reflectance at the top of atmosphere, images from different sensors and different satellites can be used to create the cloud free images. In this case, the only difference in sensors that have to be considered is their respective response curve at each band. Further tests could indicate if this effect is significant.

5. Acknowledgments

6. References

Gonzalez, R. C. and Woods, R. E. Digital image processing prentice hall. **Upper Saddle River, NJ**, 2002.

Richards, J. A. **Remote sensing digital image analysis**. Berlin et al.: Springer, 1999.

Zhu, Z. and Woodcock, C. E. Object-based cloud and cloud shadow detection in Landsat imagery. **Remote Sensing of Environment**, v. 118, p. 83-94, 2012.

Zhu, Z., Wang, S. and Woodcock, C. E. Improvement and expansion of the Fmask algorithm: cloud, cloud shadow, and snow detection for Landsats 4–7, 8, and Sentinel 2 images. **Remote Sensing of Environment**, v. 159, p. 269-277, 2015.

Frantz, D., Röder, A., Udelhoven, T., and Schmidt, M. Enhancing the detectability of clouds and their shadows in multitemporal dryland Landsat imagery: Extending Fmask. **IEEE Geoscience and Remote Sensing Letters**, v. 12, n. 6, p. 1242-1246, 2015.

Szeliski, R. Image alignment and stitching: A tutorial. **Foundations and Trends® in Computer Graphics and Vision**, v. 2, n. 1, p. 1-104, 2006.

Fonseca, L. M. G., Prasad, G. S. S. D., and Mascarenhas, N. D. A. Combined interpolation—restoration of Landsat images through FIR filter design

techniques. **International Journal of Remote Sensing**, v. 14, n. 13, p. 2547-2561, 1993.

Pinto, C., Ponzoni, F., Castro, R., Leigh, L., Mishra, N., Aaron, D., and Helder, D. First in-Flight Radiometric Calibration of MUX and WFI on-Board CBERS-4. **Remote Sensing**, v. 8, n. 5, p. 405, 2016.

Cordeiro, J. P. C., Câmara, G., De Freitas, U. M., and Almeida, F. Yet another map algebra. **Geoinformatica**, v. 13, n. 2, p. 183-202, 2009.